



This is a repository copy of *Fabrication of Nanometer and Micrometer Scale Protein Structures by Site-Specific Immobilization of Histidine-Tagged Proteins to Aminosiloxane Films with Photoremovable Protein-Resistant Protecting Groups*.

White Rose Research Online URL for this paper:  
<http://eprints.whiterose.ac.uk/94715/>

---

**Article:**

Xia, S., Cartron, M., Morby, J. et al. (3 more authors) (2016) Fabrication of Nanometer and Micrometer Scale Protein Structures by Site-Specific Immobilization of Histidine-Tagged Proteins to Aminosiloxane Films with Photoremovable Protein-Resistant Protecting Groups. *Langmuir*. ISSN 1520-5827

<https://doi.org/10.1021/acs.langmuir.5b04368>

---

© 2016 American Chemical Society. ACS AuthorChoice - This is an open access article published under an ACS AuthorChoice ([http://pubs.acs.org/page/policy/authorchoice\\_termsfuse.html](http://pubs.acs.org/page/policy/authorchoice_termsfuse.html)) which permits copying and redistribution of the article or any adaptations for non-commercial purposes.

**Reuse**

Unless indicated otherwise, fulltext items are protected by copyright with all rights reserved. The copyright exception in section 29 of the Copyright, Designs and Patents Act 1988 allows the making of a single copy solely for the purpose of non-commercial research or private study within the limits of fair dealing. The publisher or other rights-holder may allow further reproduction and re-use of this version - refer to the White Rose Research Online record for this item. Where records identify the publisher as the copyright holder, users can verify any specific terms of use on the publisher's website.

**Takedown**

If you consider content in White Rose Research Online to be in breach of UK law, please notify us by emailing [eprints@whiterose.ac.uk](mailto:eprints@whiterose.ac.uk) including the URL of the record and the reason for the withdrawal request.



[eprints@whiterose.ac.uk](mailto:eprints@whiterose.ac.uk)  
<https://eprints.whiterose.ac.uk/>

# Fabrication of Nanometer and Micrometer Scale Protein Structures by Site-Specific Immobilization of Histidine-Tagged Proteins to Aminosiloxane Films with Photoremovable Protein-Resistant Protecting Groups

*Sijing Xia,<sup>1</sup> Michaël Cartron,<sup>2</sup> James Morby,<sup>2</sup> Donald A. Bryant,<sup>3,4</sup> C. Neil Hunter<sup>2</sup> and Graham J. Leggett<sup>1</sup>*

<sup>1</sup>Department of Chemistry, University of Sheffield, S3 7HF, United Kingdom; <sup>2</sup>Department of Molecular Biology and Biotechnology, University of Sheffield, Western Bank, Sheffield S10 2TN, United Kingdom; <sup>3</sup>Department of Biochemistry and Molecular Biology, The Pennsylvania State University, University Park, PA 16802, USA; <sup>4</sup>Department of Chemistry and Biochemistry, Montana State University, Bozeman, MT 59717 USA.

## ABSTRACT

The site-specific immobilization of histidine-tagged proteins to patterns formed by far-field and near-field exposure of films of aminosilanes with protein-resistant photolabile protecting groups is demonstrated. After deprotection of the aminosilane, either through a mask or using a scanning

near-field optical microscope, the amine terminal groups are derivatized first with glutaraldehyde and then with N-(5-amino-1-carboxypentyl)iminodiacetic acid to yield a nitrilo triacetic acid (NTA) terminated surface. After complexation with  $\text{Ni}^{2+}$ , this surface binds histidine-tagged GFP and CpcA-PEB in a site-specific fashion. The chemistry is simple and reliable, and leads to extensive surface functionalization. Bright fluorescence is observed in fluorescence microscopy images of micrometer- and nanometer-scale patterns. X-ray photoelectron spectroscopy is used to study quantitatively the efficiency of photodeprotection and the reactivity of the modified surfaces. The efficiency of the protein binding process is investigated quantitatively by ellipsometry and by fluorescence microscopy. We find that regions of the surface not exposed to UV light bind negligible amounts of His-tagged proteins, indicating that the oligo(ethylene glycol) adduct on the nitrophenyl protecting group confers excellent protein resistance; in contrast, exposed regions bind His-GFP very effectively, yielding strong fluorescence that is almost completely removed on treatment of the surface with imidazole, confirming a degree of site-specific binding in excess of 90%. This simple strategy offers a versatile generic route to the spatially selective site-specific immobilization of proteins at surfaces.

## INTRODUCTION

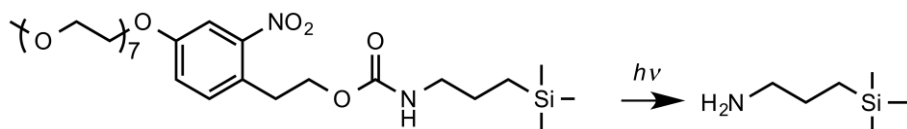
Proteins regulate many interfacial processes, including cellular attachment,<sup>1-4</sup> biosensing,<sup>5-8</sup> thrombogenesis,<sup>9,10</sup> inflammation,<sup>11</sup> and fouling by bacteria,<sup>12</sup> algae<sup>13</sup> and marine organisms.<sup>14-16</sup> The investigation of biological interfacial phenomena requires the capacity both to characterize and also to control the organization of biological molecules, including proteins, at surfaces. For example, the fabrication of assemblies of cell adhesion molecules with spatial organization on nanometer length-scales<sup>3,4</sup> has provided insights into the clustering of integrins during the formation of focal adhesions in mammalian cell attachment; the arrangement of biological

molecules at surfaces is also important in biosensors,<sup>17</sup> and the fabrication of arrays of immobilized biological recognition elements (oligonucleotides,<sup>7</sup> antibodies, aptamers<sup>18</sup> *etc.*) is important in many high-throughput detection systems.<sup>17</sup> However, the control of organization of proteins on sub-micrometer length scales remains extremely challenging; while DNA-based biochips are widespread, the development of protein chips has been significantly slower.

A variety of techniques have been used to pattern proteins on sub-micrometer length scales, including microcontact printing,<sup>19</sup> photolithography,<sup>20-22</sup> electron beam lithography,<sup>23,24</sup> dip-pen nanolithography,<sup>25,26</sup> local oxidation techniques,<sup>27</sup> near-field lithography,<sup>28-31</sup> interferometric lithography,<sup>32-34</sup> and nanoimprinting<sup>34,35</sup>. Significant progress has been made in recent years, but there is still a need to develop simple, generic methodologies capable of widespread implementation. The development of surface chemical methods to control the architecture of the biological interface is an essential element of such methods.<sup>36,37</sup> The primary requirement is to control non-specific adhesion.<sup>38</sup> The most widely used approaches have been based around oligo(ethylene glycol) (OEG) derivatives,<sup>39</sup> including OEG-terminated monolayers of alkylthiolates,<sup>40-42</sup> alkenes<sup>43</sup> and silanes,<sup>30,32</sup> poly(ethylene glycol)<sup>39</sup> and poly(oligoethylene glycol methacrylate) brushes,<sup>44,45</sup> although other materials, for example zwitterionic poly(amino acid methacrylate) brushes,<sup>33</sup> have also been used to good effect. Once adequate control of non-specific adsorption has been achieved, it is also necessary to ensure that biomolecules are presented in an appropriate conformation, by facilitating site-specific immobilization of a high fraction of the immobilized proteins, in order to address biological hypotheses in a meaningful way. There remains a need to develop simple, generic methods to achieve this end.

Recently the synthesis of a new protein-resistant siloxane, (methoxyheptaethylene glycol)nitrophenylethoxycarbonyl-protected aminopropyltriethoxysilane (henceforth OEG-

NPEOC-APTES), was described.<sup>29</sup> This molecule consists of an aminosiloxane that is protected by a photocleavable, protein-resistant protecting group. When a film formed by the adsorption of OEG-NPEOC-APTES on silica is exposed to near-UV light, photocleavage of the nitrophenyl protecting group occurs, exposing the amine and lifting the protein-resistance of the surface (Scheme 1).



**Scheme 1.** Photodeprotection of a film formed by the adsorption of protein-resistant OEG-NPEOC-APTES on silica yields an amine-terminated surface.

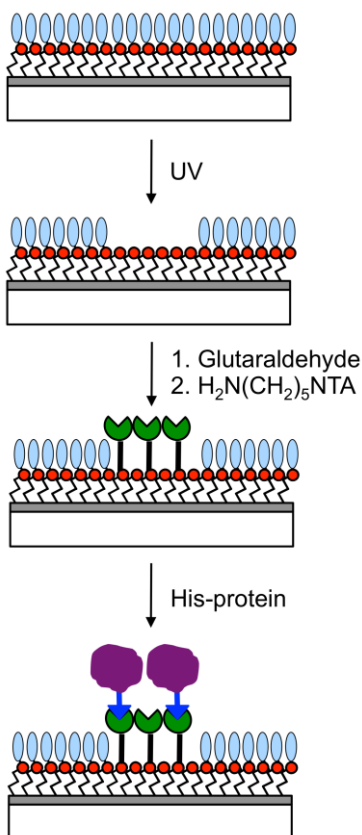


**Figure 1.** Schematic representation of the patterning process investigated here.

Here we describe an approach to the site-specific immobilization of proteins on films of OEG-NPEOC-APTES that have been patterned by exposure at 244 nm. The use of NTA-His-tag interactions to immobilize proteins at surfaces has been described by a number of authors,<sup>46-48</sup> and NTA-His-tag strategies are widely used by biochemists for the manipulation of proteins; they are thus attractive as a generic means for the control of protein organization at the nanometer scale.<sup>31,49,50</sup> The goal of the present work was to examine an approach to protein patterning that combined photopatterning of OEG-NPEOC-APTES with simple derivatization chemistry. The process, shown schematically in Figure 1, involves reaction of amine groups exposed by the lithographic step with glutaraldehyde to enable capture of a nitrilotriacetic acid (NTA) derivative with an amine linker; complexation of the NTA-functionalized surface with  $\text{Ni}^{2+}$  is followed by binding of histidine-tagged proteins. We sought to investigate quantitatively the efficacy of this simple scheme. We find that it enables the fabrication of well-resolved patterns exhibiting excellent spatial control of protein attachment, containing a high fraction of site-specifically bound proteins. We use ellipsometry and fluorescence measurements to demonstrate quantitatively the efficiency of patterning and of site-specific binding of proteins at the micrometer and nanometer length scales.

## EXPERIMENTAL

### *Materials*

Sulfuric acid ((1.83 S.G. 95+ %), hydrogen peroxide solution (100 volumes 30+ %), ammonia solution (S. G. 0.88, 35%) and toluene (HPLC grade) were supplied by Fisher Scientific (Loughborough, UK) and used as received. Ethanol (absolute) and glutaraldehyde solution (grade II, 50% in water) were obtained from VWR international (Lutterworth, UK) N-(5-amino-1-carboxypentyl)iminodiacetic acid (ABNTA) was purchased from Dojindo Molecular

Technologies (Munich, Germany). HS(CH<sub>2</sub>)<sub>11</sub>(EG)<sub>3</sub>NTA was purchased from Prochimia Surfaces (Sopot, Poland). (3-Aminopropyl)triethoxysilane (APTES, 99%) and phosphate buffered saline (PBS) tablets were supplied by Sigma-Aldrich (Poole, UK). PBS tablets were prepared into PBS buffer solution (pH = 7.4) in our lab. (Methoxyheptaethylene glycol)nitrophenylethoxycarbonyl-protected aminopropyltriethoxysilane was synthesized by AF ChemPharm Ltd (Sheffield, UK). Silicon wafers (reclaimed, p-type, <100>) were supplied by Compart Technology (Tamworth, UK). Quartz slides (50 mm × 25 mm × 1 mm) were supplied by Agar Scientific Ltd (Stansted, UK) and cover slips (20 × 60 mm) were supplied by Menzel-Gläser (Braunschweig, Germany).

All substrates used in the preparation of silane films were cleaned first with piranha solution, a mixture of 30% hydrogen peroxide and 95% concentrated sulfuric acid in the ratio of 3:7 (caution: piranha solution is a strong oxidizing agent and may detonate unexpectedly on contact with organic materials), and then with the Radio Cooperative of America (RCA) cleaning solution, a mixture of water, 30% hydrogen peroxide and 35% ammonia solution in the ratio of 5:1:1. After rinsing with copious amounts of deionized water, substrates were dried overnight in an oven at 120°C.

The gene encoding GFP was cloned into pET14b (Novagen) and the resulting plasmid was transformed into BL21 competent cells. Single colonies were inoculated into 6 mL LB plus ampicillin and allowed to grow overnight at 37°C, then subcultured into a 400 mL LB/ampicillin) in a conical flask. After shaking for 2 h at 37°C cells were induced with 1 mM IPTG for 4 h then pelleted and frozen at -20°C until further use. Cells harvested from a 400 mL culture were resuspended in 10 mL of membrane buffer A (20 mM MOPS, pH 7 100 mM NaCl), a few grains of DNase I and lysozyme and MgCl<sub>2</sub> to 20 mM were added to the suspension and left to incubate

at room temperature for one hour. The cells were then disrupted by two cycles in a French pressure cell at 18,000 psi. The lysate was centrifuged at 15,000 rpm for 25 min, and the supernatant was loaded onto a 50 mL column packed with Chelating Sepharose Fast Flow Resin (GE Healthcare) charged with nickel and equilibrated with buffer A. The column was washed with 5 column volumes of buffer A, then a gradient of 3 column volumes was applied ending with 50 ml 100% buffer B (buffer A + 500 mM imidazole). The fractions containing the pure GFP were pooled, concentrated, exchanged with buffer A then stored at  $-80^{\circ}\text{C}$  until further use.

The plasmids for the expression of CpcA-Phycoerythrobilin (CpcA-PEB) were transformed into *E. coli* BL21 (DE3) cells.<sup>51</sup> Frozen cells containing recombinant protein were thawed, re-suspended in Buffer O (20 mL of buffer was used for the cells from 1.0 L of culture), and lysed by three passages through a chilled French pressure cell at 138 MPa. The resulting whole-cell lysate was centrifuged for 35 min at 35000g to remove unbroken cells and large cellular debris. [His<sub>6</sub>]-tagged recombinant proteins were purified by affinity chromatography on columns (1.0 mL bed volume) containing Ni-Superdex-S200 resin (GE Helathcare); proteins were eluted with Buffer O containing 250 mM imidazole.<sup>52</sup> Recombinant proteins were dialyzed against buffer O overnight at  $4^{\circ}\text{C}$  to remove the imidazole. Purified proteins were stored at  $-80^{\circ}\text{C}$  until analyzed.

#### *Film Formation and Derivatization*

To prepare aminated control surfaces, clean silicon wafers or glass slides were immersed in a 1% (v/v) solution of APTES in toluene for 1 h. To prepare OEG-NPEOC-APTES films, the substrates were immersed in a 0.1% (v/v) solution of OEG-NPEOC-APTES in toluene for 48h. After film formation, the substrates were washed several times with toluene and ethanol and dried under a stream of nitrogen. Finally the samples were annealed at  $120^{\circ}\text{C}$  for 1 h in a vacuum oven.

To derivatize amine-terminated films, they were first placed in a 25% (v/v) glutaraldehyde solution (pH 5) for 1 h in order to form an aldehyde-functionalized surface. Subsequently, the samples were immersed in a 10 mM aqueous solution of ABNTA (pH 5) overnight to produce NTA functional surfaces. The Ni<sup>2+</sup>-chelated surfaces were prepared by treating NTA functional surfaces with 500 mM NiCl<sub>2</sub> for 2 h. The reaction is shown in scheme 2.

Alternatively, the aldehyde-functionalized surfaces were immersed in a 4% (v/v) solution of NH<sub>2</sub>CH<sub>2</sub>CF<sub>3</sub> in water for 3 h to produce CF<sub>3</sub> tagged surfaces. The reaction process is shown in scheme 2. Derivatization by reaction with trifluoroacetic anhydride (TFAA) was carried out by immersing samples in a 3% (v/v) solution of a 1:1 mixture of TFAA and triethylamine in DMF for 3h. After completion of the reaction, samples were rinsed with ethanol and dried under a stream of nitrogen.

Clean gold substrates were immersed in a 4mM solution of HS(CH<sub>2</sub>)<sub>11</sub>(EG)<sub>3</sub>NTA in water for 2h. The samples were rinsed with deionized water several times and dried with N<sub>2</sub>. The preparation process is shown in scheme 2.

### *Photochemistry and patterning*

Photochemical modification of silane films was carried out by exposing samples to light from a frequency-doubled argon ion laser (Coherent Innova FreD 300C) emitting at 244 nm or a HeCd laser (IK 3202R-D, Kimmon, Tokyo, Japan) emitting at 325 nm. Micropatterning was performed by exposing the sample through a copper electron microscope grid (Agar, Stansted, UK), and nanopatterning was performed using the HeCd laser coupled to a WiTec AlphaSNOM scanning near-field optical microscope (WiTec, Ulm, Germany). The SNOM system used cantilever probes (WiTec) with hollow pyramidal tips that had apertures at their apices. The resolution is defined by the aperture size, which was ca. 150 nm.

After photopatterning, OEG-NPEOC-APTES modified substrates were immersed in PBS solution (pH 7.4) for 0.5 h and dried under a stream of N<sub>2</sub> gas. Subsequently the substrates were derivatized with aldehyde functional groups and NTA as described above. Samples were immersed in a solution of the appropriate protein in phosphate buffered saline solution (pH 7.4) overnight (Scheme 2), rinsed with PBS solution and characterized using a LSM 510 Meta laser scanning confocal microscope (Carl Zeiss, Welwyn Garden City, UK)

### *Surface analysis*

X-ray photoelectron spectroscopy was carried out using a Kratos Axis Ultra X-ray photoelectron spectrometer, equipped with a delay-line detector and operating at a base pressure of  $1 \times 10^{-9}$  mbar. Survey spectra were acquired at pass energy of 160 eV, and high resolution spectra at pass energy of 20 eV. All XPS spectra were analyzed and curve-fitted using the Casa XPS software, and were corrected relative to the C 1s signal at binding energy (B.E.) = 285.0 eV. Peak fitting was done using combinations of Gaussian (30%) and Lorentzian (70%) curves. The components in a given region were constrained to have the same full width at half maximum (FWHM), in the range 1.3 – 1.5 eV. Measurements were typically made in triplicate, and errors quoted in numerical data are the standard deviations.

Film thicknesses were measured using an M-2000V ellipsometer (J. A. Woollam Co. Inc). The data were fitted using the model into a Cauchy model using the software CompleteEASE.

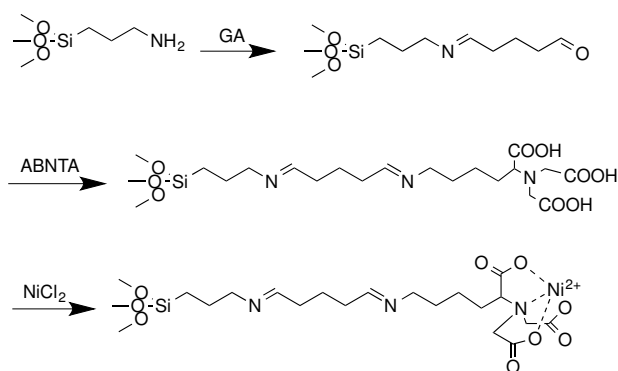
Confocal microscopy was carried out using an LSM 510 laser scanning confocal microscope (Carl Zeiss, Welwyn Garden City, UK) Lasers emitting at 488 nm (GFP) and 543 nm (CpcA-PEB) were used for excitation. A 40× or 63× magnification oil immersion lens was used for imaging the samples, which were mounted in an antifade reagent (glycerol-PBS solution, AF1)

(Citifluor Ltd., London, United Kingdom). The captured images were analyzed using Zeiss LSM image browser software.

## RESULTS AND DISCUSSION

### *XPS analysis of NTA functionalized APTES surfaces*

Scheme 2 shows the sequence of reactions used to form an NTA-functionalized surface. Deprotection of OEG-NPEOC-APTES yields aminopropyl(triethoxy silane) (APTES), which is reacted with glutaraldehyde (GA), a dialdehyde bifunctional linker. One aldehyde group on the GA molecule reacts with the terminal amine to form an imine bond, while the other aldehyde group is presented at the surface. Incubation of this aldehyde-terminated surface with N-(5-amino-1-carboxypentyl)iminodiacetic acid (ABNTA) leads to attachment of ABNTA to the surface via the formation of a new imine linkage between the amine linker and the surface-bound aldehyde. The reaction leading to the formation of the imine bond is acid-catalyzed, so the reaction is carried out at pH 5.



**Scheme 2.** Sequence of reactions used to prepare an aminated surface for immobilization of histidine-tagged proteins: reaction with glutaraldehyde to generate an aldehyde-functionalized surface; reaction between surface aldehyde groups and N-(5-amino-1-carboxypentyl)iminodiacetic acid to yield an NTA-functionalized surface; and finally complexation of the carboxylic acid groups with  $\text{Ni}^{2+}$  ions.

To characterize the reaction sequence in Scheme 2, and optimize the reaction conditions, measurements were made by XPS on APTES films. The XPS C1s high resolution spectra for different surfaces are shown in Figure 2. The spectrum of the film that results from adsorption of APTES onto silicon dioxide (Figure 2(a)) is fitted with two peaks: one with binding energy (BE) of 285.0 eV that is attributed to C–C–C and another with a BE of 286.6 eV that is attributed to C–C–N. After reaction with GA (Figure 2(b)), the spectrum of the APTES-GA surfaces is fitted with three peaks: the component at 285.0 eV again corresponds to aliphatic carbon atoms; the peak at 286.5 eV is attributed to carbon atoms in unreacted amines (C–C–N) or adjacent to the nitrogen atom in the imine group (C–C=N); and the component at 288.1 eV is attributed to C–C=O in the free aldehyde group  $\omega$  to the imine bond. After incubation of the surface with ABNTA (Figure 2(c)), a fourth component is observed at 289.0 eV that is attributed to the carboxylate carbon atom.

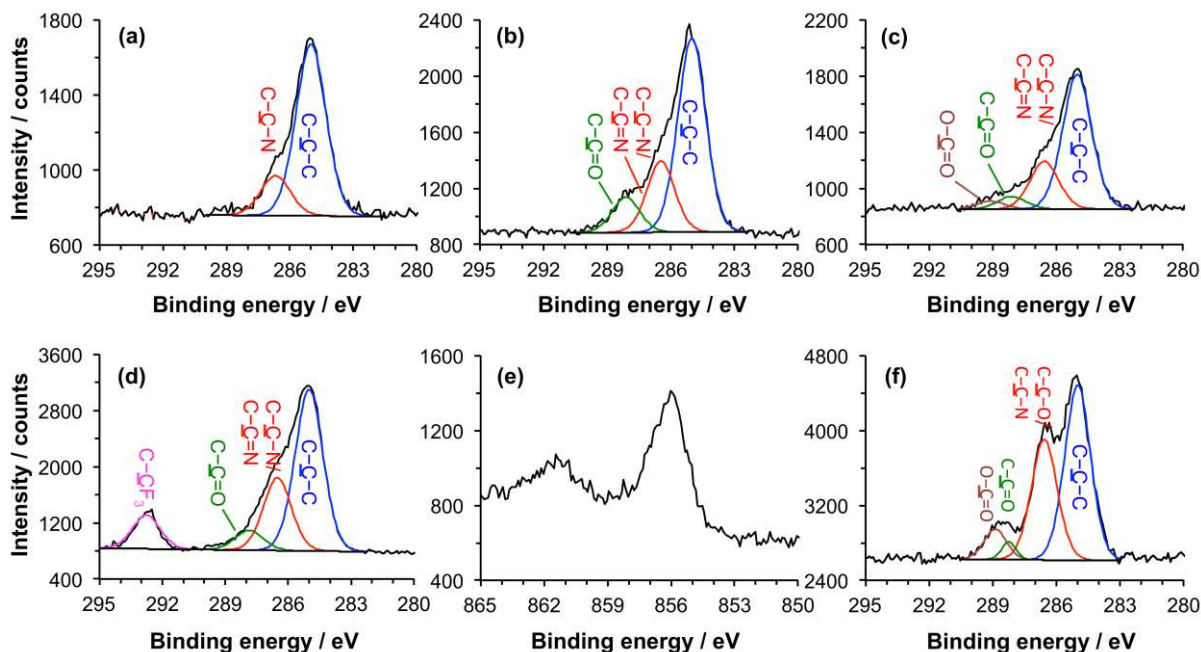


**Figure 2.** XPS data for APTES films following surface chemical reactions. (a) C1s spectrum of an as-prepared film. (b) C1s spectrum after incubation with glutaraldehyde solution. (c) C1s

spectrum after reaction of the aldehyde-functionalized surface with ABNTA. (d) C1s spectrum after reaction of the aldehyde-functionalized surface with trifluoroethylamine. (e) Ni2p spectrum after incubation of the NTA-functionalized surface with nickel chloride solution. (f) C1s reference spectrum obtained for SAM of an NTA-terminated oligo(ethylene glycol) derivatized alkylthiolate on gold.

Quantitative data extracted from the XPS spectra are shown in Table 1. For the as-prepared film of APTES, the experimentally determined fraction of C–C–N is 20%. The expected value is 33.3%. The N:C elemental ratio was 0.16, compared to a predicted value of 0.33 (see Supporting Information), consistent with this interpretation of the C1s spectrum. Aminated surfaces have comparatively high surface free energies, and it is likely that the reduced size of the C–C–N component reflects the presence at the surface of atmospheric contamination adsorbed at the surface prior to analysis. After reaction with GA, a new component was observed corresponding to the aldehydic carbon atom. The experimentally determined percentage of C=O is 11.4%, rather similar to the calculated value 12.5%. The area of the C–C–N component also has a peak area that is similar to the expected value. This implies that a high fraction of the terminal amine groups has reacted with GA. However, caution must be exercised given that the area of the C–C–N component was somewhat reduced for the as-prepared film, and it is known that contaminant species also often contain a component at ca. 286.6 eV in their C1s spectra.<sup>53</sup> The elemental data (Supporting Information) suggest that the N:C ratio is smaller than expected (0.7, compared to a calculated value of 0.13), suggesting that there may indeed be some adventitious contamination, as at the first stage in the derivatisation process. The final stage of the attachment process yields a less ambiguous indication of the net efficiency of reaction; the carboxylate component observed after attachment of ABNTA was not observed at any other stage of the process. The

area of this peak was measured to be 3.7%, compared with an expected value, assuming 100% derivatization, of 16.8%. Neglecting attenuation effects (which will influence the precise yield), these data suggest that *ca.* 25% of the APTES terminal amine groups are ultimately derivatized by NTA. Bearing in mind that the NTA group is bulky – hence the final yield will be sterically constrained – this represents a significant degree of derivatization, and the most likely explanation for the anomalous area of the C–C–N peak in Figure 2(a) is that it results from surface contamination that was not transferred through to later stages of the derivatization process.

**Table 1.** Contributions to the C1s spectra (as % of the total C1s peak area) for APTES films following surface derivatization reactions. Calculated values are given in parentheses.

	C–C–C	C–C–O, C–C–N	C–C=O, N–C=O	O–C=O, O–CN=O	C–C–F <sub>3</sub>
APTES	80 ± 2 (66.7)	20 ± 2 (33.3)	n/a	n/a	n/a
APTES + GA	64 ± 1 (62.5)	25 ± 1 (25.0)	11.4 ± 0.3 (12.5)	n/a	n/a
APTES + GA + ABNTA	66 ± 1 (44.4)	24 ± 1 (38.8)	6.8 ± 0.6 (n/a)	3.7 ± 0.4 (16.8)	n/a
APTES + GA + NH <sub>2</sub> CH <sub>2</sub> CF <sub>3</sub>	52 ± 5 (50.0)	27 ± 3 (40.0)	9 ± 3 (n/a)	n/a	11.5 ± 0.3 (10.0)
HS(CH <sub>2</sub> ) <sub>11</sub> EG <sub>3</sub> NT A	54 ± 1 (44.9)	36 ± 1 (41.4)	3.3 ± 0.6 (3.4)	8.2 ± 0.4 (10.3)	n/a

To test this hypothesis, a further reaction was carried out using trifluoroethylamine, a small molecule with a distinctive fluorinated label, in place of ABNTA (Figure 2(d)). For this molecule, the area of the CF<sub>3</sub> component in the XPS spectrum after reaction with the GA-functionalized APTES film was 11.5%, slightly larger than the calculated value of 10% for

complete reaction. This result suggests that the extent of derivatization is very high, and that the sequence of steps involved in Scheme 2 is highly efficient. The fact that the yield appears to be greater than 100% is explained by attenuation effects: the trifluoromethyl group is located at the top of the monolayer and the signal is less strongly attenuated than, for example, photoelectrons emitted from the vicinity of the imine bond. The high extent of reaction achieved here is consistent with the hypothesis that the final extent of derivatization by ABNTA is limited by steric constraints.

Binding of His-tagged proteins requires the coordination of  $\text{Ni}^{2+}$  to the NTA-terminated film. To quantify the efficiency of this chelation process, samples were immersed in a 500 mM aqueous solution of  $\text{NiCl}_2$  for 2 h and characterized by XPS. The observation of a peak in the Ni2p high resolution spectrum (Figure 2(e)) confirmed, qualitatively, the chelation of  $\text{Ni}^{2+}$  to the NTA groups. The experimental composition of nickel, determined from the survey spectrum (supporting information), was 0.7%, from which the chelating efficiency of ABNTA units was estimated to be ca. 0.5 Ni atoms per chelator (the theoretical value is 1).

In order to verify the positions of the components in the C1s spectra, self-assembled monolayers formed by the adsorption of HS-C<sub>11</sub>-(EG)<sub>3</sub>-NTA on gold were used as a reference, as described previously by Cheng et al.<sup>54</sup> The C1s spectrum of the SAMs was also fitted with four peaks (Figure 2(f)): 285.0 eV attributed to C-C-C; 286.6 eV attributed to C-C-O and C-N; 288.2 eV attributed to N-C=O; and 288.9 eV attributed to O-C=O. Comparing this C1s spectrum (figure 2(f)) with the one for the APTES-GA-NTA surface (figure 2(c)), we find that they have peaks with almost the same BE for O-C=O, although the relative areas are different because of the different compositions of the adsorbate molecules.

From all the results above, it was concluded that an NTA-functionalized surface had been prepared successfully on the APTES film.

*XPS analysis of NTA functionalized OEG-NPEOC-APTES surfaces*

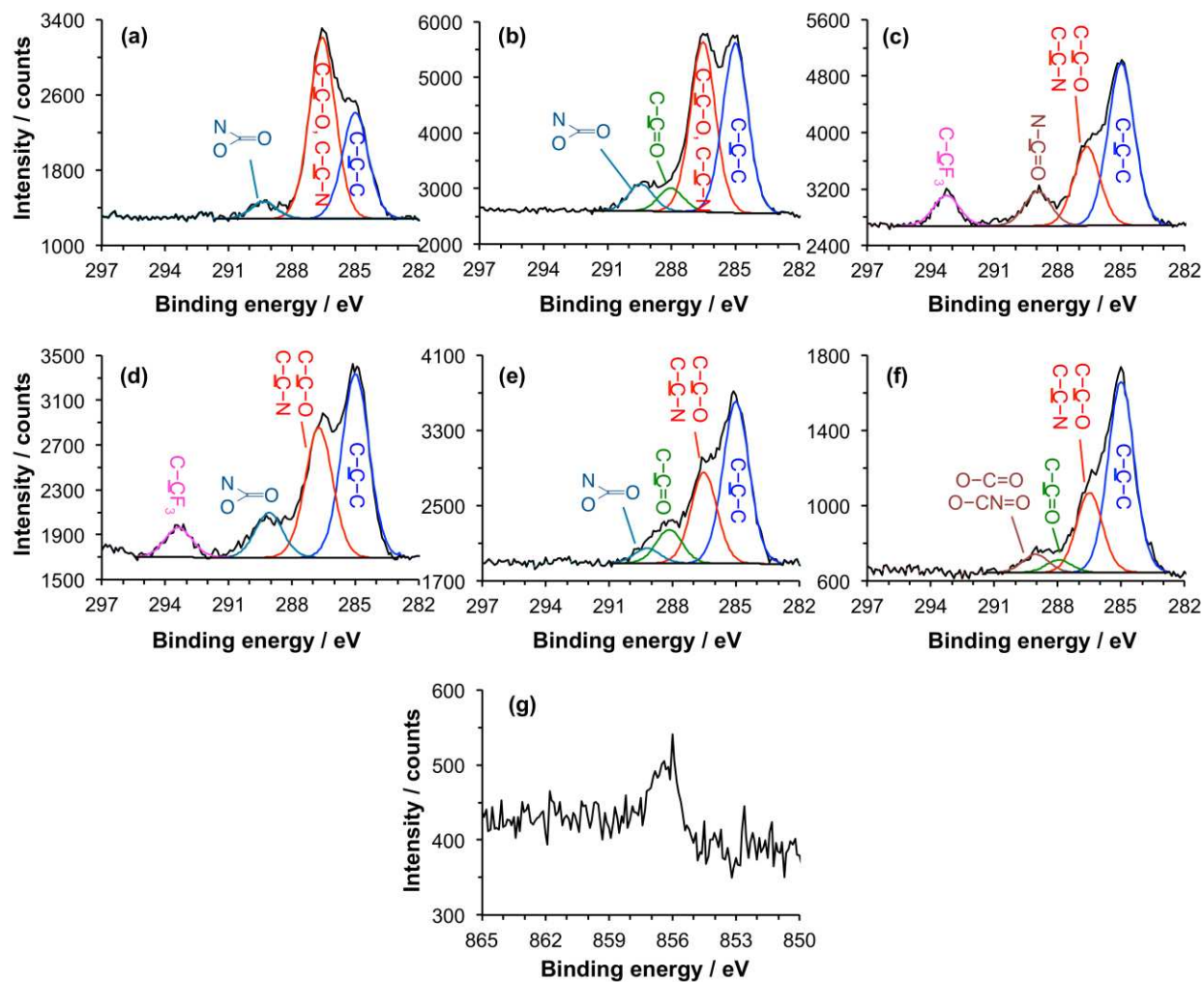


**Figure 3.** (a) C1s spectrum of an as-prepared OEG-NPEOC-APTES film. (b) C1s spectrum after photodeprotection by exposure to UV light at 244 nm and immersion in PBS solution. (c) and (d) C1s spectra of, respectively, an APTES film and a deprotected OEG-NPEOC-APTES film following derivatization by reaction with TFAA. (e) C1s spectrum of a deprotected OEG-NPEOC-APTES film after incubation with glutaraldehyde solution; (f) C1s spectrum acquired after subsequent reaction of the aldehyde-functionalized surface with ABNTA. (g) Ni2p

spectrum after incubation of an NTA-functionalized surface similar to that in (f) with nickel chloride solution.

The XPS C1s spectrum of a freshly prepared film of OEG-NPEOC-APTES is shown in Figure 3(a). The most intense component in the fitted spectrum is the one at 286.5 eV corresponding to the ether carbon atoms in the OEG-functionalized protecting group. Carbon adjacent to nitrogen yields a slightly smaller chemical shift but contributes to the size of this peak. A smaller hydrocarbon peak is observed at 285.0 eV, corresponding to photoemission from carbon atoms in the aromatic ring and in the propyl linker. Finally, a small peak at 289.3 eV is attributed to the carbamate carbon, which is doubly bonded to oxygen and singly bonded to both oxygen and nitrogen.

Samples were exposed to UV light. Alang Ahmad et al reported that freshly prepared films of NPEOC-APTES yield two components in the N1s region of the XPS spectrum, corresponding to the carbamate nitrogen atom and the nitrogen in the NO<sub>2</sub> group,<sup>55</sup> near-UV UV exposure led to deprotection of OEG-NPEOC-APTES, accompanied by loss of the NO<sub>2</sub> component in the N1s spectrum. In the present work, the NO<sub>2</sub> component was also found to have disappeared after exposure at the dose of 15 J cm<sup>-2</sup> at 244nm, but the C1s spectrum (Figure 3(b)) retained a significant component at 286.6 eV. While the carbon atom adjacent to N in the propyl chain was included in this component in Figures 2(a) and 3(a), the size of this component is nevertheless somewhat larger than expected in Figure 3(b). This suggests that a significant amount of the oligo(ethylene glycol) adduct remains at the surface, although relative to the component at 285.0 eV it is reduced in size. A third component is observed at 288.1 eV and attributed, tentatively, to carbonyl carbon atoms. One possibility is that at the large exposure and high photon energy used here, some of the OEG adducts undergo photodegradation to yield aldehydes, as has been

reported elsewhere for similar materials.<sup>30,56</sup> To test this hypothesis, samples that had been exposed to UV light were incubated with trifluoroethylamine, a reagent shown previously to react with aldehydes produced in photodegradation of OEG-terminated monolayers<sup>57</sup>. Over the range of exposure studied here, there was no uptake of fluorine by the samples, suggesting that photodegradation of the OEG groups to yield aldehydes was not occurring. Finally, a peak is also observed at 289.0 eV that is attributed to carbamate carbon atoms.

**Table 2.** Contributions to the C1s spectra (as % of the total C1s peak area) for OEG-NPEOC-APTES before and after photodeprotection, and after derivatization. Calculated values are given in parentheses

	C-C-C	C-C-O, C-C-N	C-C=O, N-C=O	O-C=O, O-CN=O	C-C-F <sub>3</sub>
OEG-NPEOC-APTES	34 ± 2 (25.9)	61 ± 2 (70.4)	n/a	5.2 ± 0.4 (3.7)	n/a
Deprotected OEG-NPEOC-APTES	42 ± 2 (66.7)	45 ± 2 (33.3)	n/a	n/a	n/a
Deprotected film + TFAA	47 ± 1 (40.0)	34 ± 1 (20.0)	13 ± 1 (20.0)	n/a	7 ± 1 (20.0)
Deprotected film + GA	51 ± 2 (62.5)	33 ± 3 (25.0)	11 ± 1 (12.5)	n/a	n/a
Deprotected film + GA + ABNTA	62 ± 1 (44.4)	27 ± 1 (38.9)	3.8 ± 0.4 (n/a)	7.1 ± 0.8 (16.7)	n/a

Based on these data we summarize the photochemistry of OEG-NPEOC-APTES as follows: at high exposures, N1s spectra suggest that all of the NO<sub>2</sub> groups are lost, but C1s spectra suggest that OEG groups remain at the surface (albeit at slightly reduced concentrations). We hypothesize the following explanation. Photodeprotection occurs at 244 nm, as described by Alang Ahmad et al at longer wavelengths,<sup>29</sup> but a competing reaction occurs after exposure at

244 nm that leads to conversion of the nitro group to a nitroso group rather than cleavage of the C-N bond in the carbamate group. This competing reaction has been reported by a number of researchers in studies of nitrophenyl protecting groups.<sup>58</sup>

To quantify the extent of photodeprotection further, a model reaction was utilized. First, as a control, films formed by the adsorption of APTES on glass were reacted with trifluoro(acetic anhydride) (TFAA). The resulting C1s spectrum is shown in Figure 3(c). As expected, reaction between the anhydride and the amine group of the adsorbate yields new components corresponding to the amide carbon (289.3 eV) and the carbon atom in the trifluoromethyl group (293.7 eV). These latter components are in the ratio 1:1, indicative of extensive derivatization. Second, films formed from OEG-NPEOC-APTES were exposed to UV light and were also reacted with TFAA. The resulting C1s spectrum is shown in Figure 3(d). A peak corresponding to the carbon atom in the trifluoromethyl group is observed clearly. The ratio of the area of this peak to that of the main hydrocarbon peak at 285 eV is similar to that in Figure 3(c). A peak is also observed at 289.3 eV that includes contributions from both the carbamate group of any adsorbates with intact protecting groups, and also the carbonyl groups of deprotected, derivatized adsorbates. The ratio of the intensity of the CF<sub>3</sub> component to this peak provides a direct measure of the extent of derivatization by TFAA and, hence, of the progress of the photodeprotection reaction to completion. Data are shown in Figure 4 as a function of UV exposure. The limiting value of the intensity of the CF<sub>3</sub> component corresponds to a film in which ca. 70% of the adsorbates have been deprotected and derivatized by reaction with TFAA. Based on these data we conclude that it is likely that a side reaction occurs. The nature of this side reaction is not established definitively. However, one possibility is the conversion of the nitro group to a nitroso group, as has been reported previously.<sup>58</sup> In support of this, an

unexpected additional component was observed at ca. 402 eV in the N1s spectrum after UV exposure (see Supporting Information), consistent with some literature reports of XPS spectra of nitroso compounds.<sup>59</sup> However, the majority of adsorbates – *ca.* two thirds at exposures of 5 J cm<sup>-2</sup> and higher – undergo deprotection to expose their amine groups for subsequent reaction.

UV-modified OEG-NPEOC-APTES films were reacted with GA (Figure 3(e)) and then with ABNTA (Figure 3(d)). After reaction with GA, the C1s spectrum was much closer to the spectrum acquired for APTES after reaction with GA (Figure 2(b)). The component at 286.6 eV was slightly increased in size, and a small component was still observed that was due to the carbamate. After reaction with ABNTA, the spectrum obtained for the deprotected OEG-NPEOC-APTES film was very similar indeed to that obtained after derivatization of APTES. Again, the component at 286.6 eV was larger, and the peak at 289.4 eV is slightly larger in Figure 3(f) than the corresponding peak in Figure 2(c) (7.1 and 3.7 %, respectively). Complexation with Ni<sup>2+</sup> yielded an Ni2p peak, indicative of formation of the desired nickel-NTA complex.

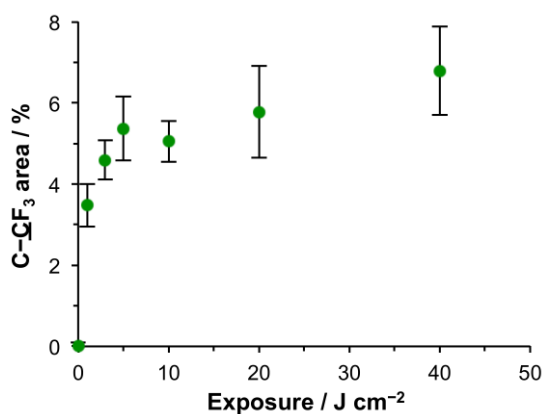


**Figure 4.** Variation in the C-CF<sub>3</sub> peak area (as a percentage of the total C1s peak area) as a function of UV exposure at 244 nm for OEG-NPEOC-APTES films following derivatization with TFAA.

In summary, XPS data suggest that the photochemistry of OEG-NPEOC-APTES is more complex at 244 eV than was previously described at near-UV wavelengths. A competing reaction likely occurs that involves conversion of the nitro group to a nitroso group, inhibiting deprotection. However, deprotection is extensive at exposures  $> 5 \text{ J cm}^{-2}$  yielding amine groups that are derivatized by GA, to yield surface aldehydes that react with ABNTA. The ultimate efficiency of attachment of ABNTA (as gauged by the area of the carboxylate component in the C1s spectrum) is slightly greater than that obtained for the control surface, APTES.

#### *Binding of His-Tagged Proteins*

In order to quantify the relationship between the UV exposure and immobilization of His-tagged protein, the adsorption of two His-tagged fluorescent proteins was studied using ellipsometry. Figure 5(a) shows the variation in the thickness of the adsorbed layer for two His-GFP and His-CpcA-PEB as a function of UV exposure on NTA functionalized OEG-NPEOC-APTES surfaces. The ellipsometric thickness is proportional to the amount of adsorbed protein. The dimensions of GFP are ca.  $24 \text{ \AA} \times 24 \text{ \AA} \times 42 \text{ \AA}$ , and those of CpcA are ca.  $24 \text{ \AA} \times 36 \text{ \AA} \times 67 \text{ \AA}$ . The thickness of a monolayer will thus depend upon the presentation of the protein at the surface. It can be seen from Figure 5(a) that for both proteins, the adsorbed amount increases up to an exposure of  $5 \text{ J cm}^{-2}$ . Subsequently, the thickness of the protein layer changes very little. The final thickness value of GFP is ca.  $35 \text{ \AA}$  and that of CpcA-PEB-PEB is ca.  $40 \text{ \AA}$ . These data suggest that an exposure of  $5 \text{ J cm}^{-2}$  is sufficient to ensure the formation of a monolayer of site-specifically oriented protein, and that the thickness of the two proteins is similar when site-specifically bound via the His-tag.

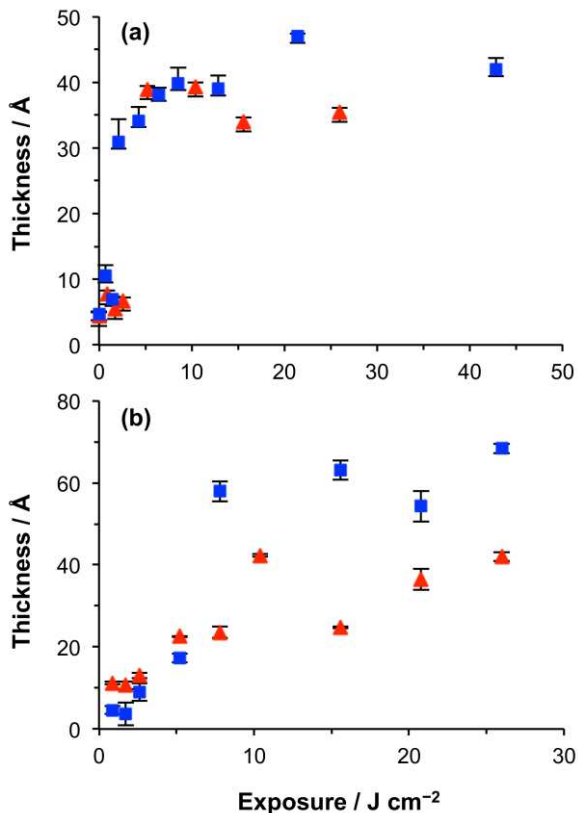


**Figure 5.** Ellipsometric measurements of the thickness of the adsorbed layer of GFP (red triangles) and CpcA-PEB-PEB (blue squares) on films of OEG-NPEOC-APTES as a function of UV exposure (a) after treatment with GA/ABNTA/Ni<sup>2+</sup> to create an NTA-functionalized surface and (b) without any post-exposure modification.

The amount of protein adsorbed at the surface was measured by ellipsometry as a function of UV exposure for samples that were not derivatized with ABNTA (figure 5(b)). The thickness of the adsorbed layer increased more slowly, and reached a limiting value for each protein after an exposure of ca. 10 J cm<sup>-2</sup>. The limiting thickness of the GFP layer is ca. 40 Å, while that of CpcA-PEB-PEB is ca. 65 Å. The increased thickness of the monolayer that forms by adsorption of CpcA-PEB-PEB may reflect the fact that the protein is oriented differently at the surface.

### *Protein patterning*

Samples of OEG-NPEOC-APTES were exposed to UV light through a mask and treated with GA, ABNTA and Ni<sup>2+</sup>, then incubated in solutions of His-GFP and His-CpcA-PEB-PEB. Figures 6(a) and (b) show confocal fluorescence images of the resulting micropatterns. Bright fluorescence is observed for the exposed regions (squares) indicating high levels of attachment, and dark contrast regions in the masked areas (bars) indicated low levels of nonspecific protein adsorption on the unexposed regions where the OEG-NPEOC protecting groups were intact. The size of the squares with protein is *ca.* 20 × 20 μm<sup>2</sup> and the width of the dark bars is *ca.* 10 μm.

Nanofabrication was carried out by near-field lithography. For these experiments, an HeCd laser (325 nm) was coupled to a scanning near-field optical microscope because the optics of the microscope were not transparent at 244 nm. The probe was traced across the OEG-NPEOC-APTES modified surfaces to fabricate a series of 6 parallel lines, the exposed regions were functionalized with NTA and Ni<sup>2+</sup> and the samples were immersed in solutions of His-GFP or His-CpcA-PEB-PEB to facilitate binding of the proteins to the features modified by exposure to the near field. Figure 6(c) and (d) show confocal fluorescence images of GFP and CpcA-PEB-PEB nanopatterns. Strong fluorescence contrast was observed between the lines and the unexposed regions. Line cross sections through the nanopatterns demonstrate that sharp and well-defined features have been formed (figure 6(e, f)). In the regions to which the proteins were attached, the fluorescence signal was as high as 250 a.u. for GFP (figure 6(e)) and 200 a.u. for CpcA-PEB-PEB (figure 6(f)), similar to values obtained for micropatterned samples, and the signal in the between the lines was close to zero, indicating good spatial control of protein attachment. A small number of isolated spots is also observed between the lines fabricated by near-field lithography; we speculate that these may result from adventitious deposition of small aggregates of protein that formed in solution.

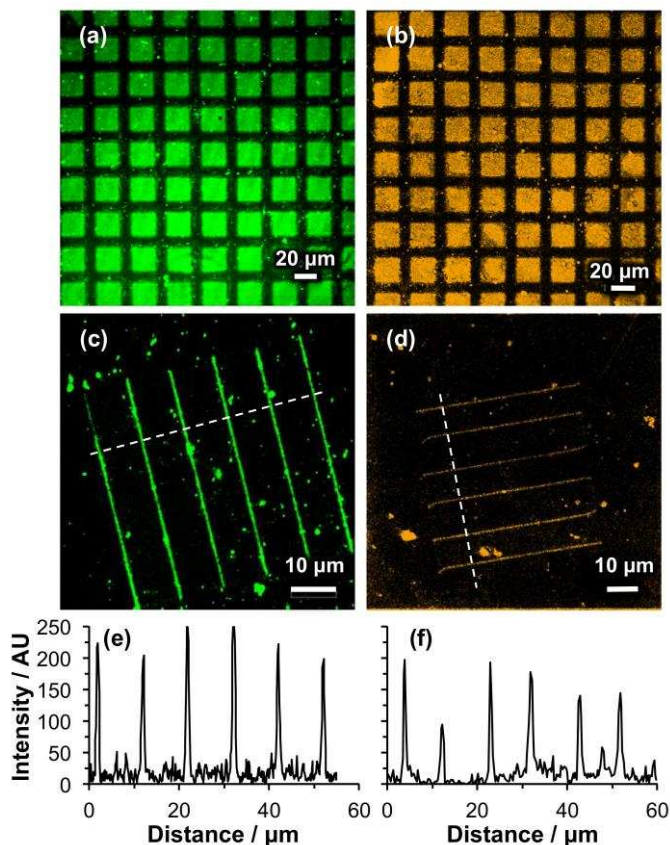


**Figure 6.** Confocal fluorescence microscopy images of patterned samples formed by exposure of OEG-NPEOC-APTES through a mask (a, b) and using a near-field probe (c, d) prior to activation of the surface by incubation with GA, ABNTA and then  $\text{Ni}^{2+}$ . Images (a) and (c) show samples to which His-GFP has been bound, and samples (b) and (d) show samples to which His-CpcA-PEB-PEB has been bound. Representative line sections, measured along the dashed lines marked in (c) and (d), are shown in (e) and (f).

#### *Site-Specific Attachment of Proteins to Patterned Samples*

An OEG-NPEOC-APTES film sample was exposed to UV light through a mask. In exposed regions the adsorbates are expected to undergo deprotection to expose amine groups that may be activated using GA, and coupled to ABNTA. After complexation of the NTA-derivatized regions with  $\text{Ni}^{2+}$ , the sample was immersed in a solution of His-tagged GFP. After rinsing, the sample

was imaged using confocal fluorescence microscopy (Figure 7(a)). Square regions of bright fluorescence may be observed. These correspond to regions that were exposed to UV light during the patterning step; the observation of bright fluorescence from these regions confirms that the protein has been immobilized successfully. The dark bars correspond to regions that were masked during exposure. The low fluorescence intensity in those regions (no more than background noise) demonstrates the excellent protein resistance of the OEG-terminated as-prepared surface.

To test whether the immobilized proteins were site-specifically bound, the sample was treated with a large excess of imidazole, which removes  $\text{Ni}^{2+}$  from the His-tagged protein/ $\text{Ni}^{2+}$ /NTA complex via ligand competition and disrupts the bond between the His-tag and the NTA group. Figure 7(b) shows a confocal fluorescence micrograph of the sample imaged in Figure 7(a) after the addition of 1M imidazole. The dramatic reduction in fluorescence intensity confirms that the majority of the protein has been displaced, and indicates that the protein that was imaged in Figure 7(a) was largely bound in a site-specific fashion to the surface. Comparisons of line-sections through the two images indicates a very low level of residual fluorescence due to non-specifically bound protein, and some bright spots in Figure 7(b) are due to immovable spots that are attributed to nonspecific binding.

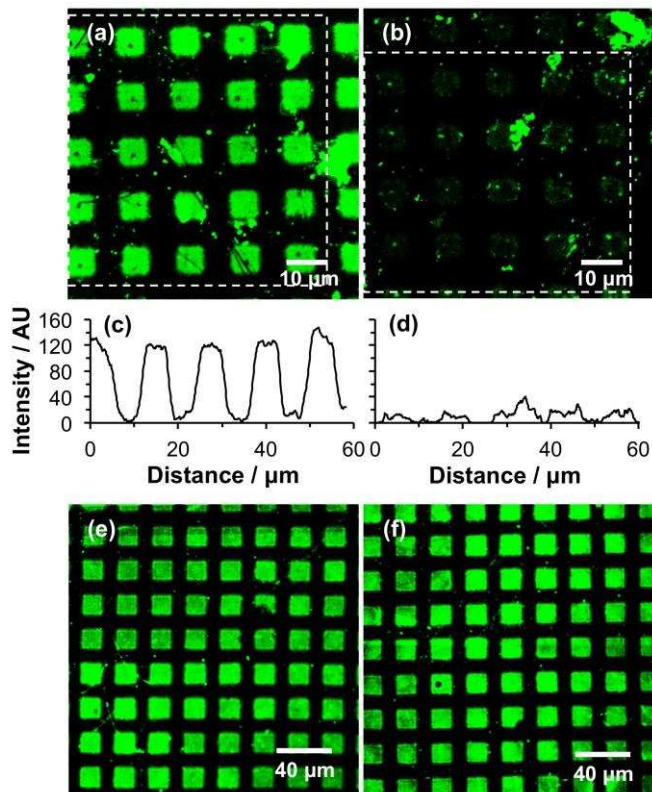


**Figure 7.** (a) Confocal fluorescence micrograph of an OEG-NPEOC-APTES film sample following UV exposure through a mask, derivatization with ABNTA/ $\text{Ni}^{2+}$  and immersion in a solution of His-tagged GFP. (b) Micrograph of the same sample following subsequent treatment with a 1 M solution of imidazole in water. (c) and (d) Sections averaged across the regions indicated by the dashed boxes in (a) and (b), respectively. (c) Fluorescence image of an OEG-NPEOC-APTES film exposed to UV light, using the same exposure employed to prepare the sample in (a), but without subsequent derivatization by NTA, after immersion in a solution of His-GFP. (d) Fluorescence micrograph of the sample shown in (c) after treatment with a 1 M solution of imidazole.

Repetition of the experiment in the absence of the GA/ABNTA/ $\text{Ni}^{2+}$  activation steps leads to His-GFP adsorption onto the patterned surface, resulting in bright fluorescence from exposed areas of the sample (Figure 7(c)). However, in contrast to the behavior seen in Figure 7(b), this

fluorescence is not diminished when the sample is treated with a 1 M solution of imidazole. Hence, in the absence of the GA/ABNTA/Ni<sup>2+</sup> activation steps the protein is able to adsorb in a non-specific fashion to the surface.

## CONCLUSIONS

Exposure of aminosilane films protected with an oligo(ethylene glycol) nitrophenyl group by irradiation at 244 nm leads to photodeprotection, exposing amine groups with an efficiency of *ca.* 70% within the XPS sampling depth. The reaction does not proceed to completion because of a side reaction, which likely leads to conversion of the nitro group in the protecting group to a nitroso group. The remaining surface remains moderately protein-resistant because the side reaction leads to retention of some of the oligo(ethylene glycol) adducts. Deprotected films are reacted first with glutaraldehyde and second with aminobutyl nitrilotriacetic acid, yielding a surface carboxylate concentration slightly exceeding that achieved for an aminosilane control. The resulting surfaces may be complexed with Ni<sup>2+</sup> to facilitate efficient site-specific immobilization of His-tagged proteins. Micrometer- and nanometer-scale patterns may be formed when the exposure is carried out either using a mask or a near-field probe. Treatment of the resulting patterns with 1 M imidazole leads to almost quantitative removal of the immobilized protein, demonstrating that the protein attachment process is extremely selective. Site-specific binding of two different His-tagged proteins is demonstrated. This system appears to provide a convenient generic approach to the site-specific immobilization of proteins in micrometer- and nanometer-scale assemblies.

**Supporting Information Available:** elemental composition data obtained from XPS spectra and N1s spectra of OEG-NPEOC-APTES before and after exposure to UV light. This material is available free of charge via the Internet at <http://pubs.acs.org>.

## ACKNOWLEDGEMENTS

The authors are grateful to EPSRC (Grant EP/I012060/1) for financial support. SX Thanks the University for a Research Scholarship. CNH and MJD gratefully acknowledge financial support from the Biotechnology and Biological Sciences Research Council (BBSRC UK), award number BB/M000265/1. CNH was also supported by an Advanced Award 338895 from the European Research Council. JM was supported by a BBSRC doctoral studentship. This work was also supported as part of the Photosynthetic Antenna Research Center (PARC), an Energy Frontier Research Center funded by the U.S. Department of Energy, Office of Science, Office of Basic Energy Sciences under Award Number DE-SC 0001035. PARC's role was to provide partial support for DAB and CNH.

## REFERENCES

- (1) Lopez, G. P.; Albers, M. W.; Schreiber, S. L.; Carroll, R.; Peralta, E.; Whitesides, G. M. Convenient Methods for Patterning the Adhesion of Mammalian Cells to Surfaces using Self-Assembled Monolayers of Alkanethiolates on Gold. *J. Am. Chem. Soc.* **1993**, *115*, 5877-5878.
- (2) Chen, C. S.; Mrksich, M.; Huang, S.; Whitesides, G. M.; Ingber, D. E. Geometric Control of Cell Life and Death. *Science* **1997**, *276*, 1425-1428.
- (3) Cavalcanti-Adam, E. A.; Volberg, T.; Micoulet, A.; Kessler, H.; Geiger, B.; Spatz, J. P. Cell Spreading and Focal Adhesion Dynamics are Regulated by Spacing of Integrin Ligands. *Biophys. J.* **2007**, *92*, 2964-2974.

- (4) Cavalcanti-Adam; A., E.; Micoulet, A.; Blümmel, J.; Auernheimer, J.; Kessler, H.; Spatz, J. P. Lateral Spacing of Integrin Ligands Influences Cell Spreading and Focal Adhesion Assembly. *Eur. J. Cell Biol.* **2006**, *85*, 219-224.
- (5) Tamura, T.; Hamachi, I. Tamura, T.; Hamachi, I. Recent Progress in Design of Protein-Based Fluorescent Biosensors and Their Cellular Applications. *ACS Chem. Biol.* **2014**, *9*, 2708-2717.
- (6) Turner, A. P. F. Biosensors: Sense and Sensibility. *Chem. Soc. Rev.* **2013**, *42*, 3184-3196.
- (7) Zhao, W.-W.; Xu, J.-J.; Chen, H.-Y. Photoelectrochemical DNA Biosensors. *Chem. Rev.* **2014**, *114*, 7421-7441.
- (8) Liu, Q.; Wu, C.; Cai, H.; Hu, N.; Zhou, J.; Wang, P. Cell-Based Biosensors and Their Application in Biomedicine. *Chem. Rev.* **2014**, *114*, 6423-6461.
- (9) Leslie, D. C.; Waterhouse, A.; Berthet, J. B.; Valentin, T. M.; Watters, A. L.; Jain, A.; Kim, P.; Hatton, B. D.; Nedder, A.; Donovan, K.; Super, E. H.; Howell, C.; Johnson, C. P.; Vu, T. L.; Bolgen, D. E.; Rifai, S.; Hansen, A. R.; Aizenberg, M.; Super, M.; Aizenberg, J.; Ingber, D. E. A Bioinspired Omniphobic Surface Coating on Medical Devices Prevents Thrombosis and Biofouling. *Nat. Biotech.* **2014**, *32*, 1134-1140.
- (10) Fedorov, K.; Blaszykowski, C.; Sheikh, S.; Reheman, A.; Romaschin, A.; Ni, H.; Thompson, M. Prevention of Thrombogenesis from Whole Human Blood on Plastic Polymer by Ultrathin Monoethylene Glycol Silane Adlayer. *Langmuir* **2014**, *30*, 3217-3222.

- (11) Rostam, H. M.; Singh, S.; Vrana, N. E.; Alexander, M. R.; Ghaemmaghami, A. M. Impact of Surface Chemistry and Topography on the Function of Antigen Presenting Cells. *Biomater. Sci.* **2015**, *3*, 424-441.
- (12) Banerjee, I.; Pangule, R. C.; Kane, R. S. Antifouling Coatings: Recent Developments in the Design of Surfaces That Prevent Fouling by Proteins, Bacteria, and Marine Organisms. *Adv. Mater.* **2011**, *23*, 690-718.
- (13) Ge, S.; Agbakpe, M.; Wu, Z.; Kuang, L.; Zhang, W.; Wang, X. Influences of Surface Coating, UV Irradiation and Magnetic Field on the Algae Removal Using Magnetite Nanoparticles. *Environ. Sci. Technol.* **2015**, *49*, 1190-1196.
- (14) Rosenhahn, A.; Schilp, S.; Kreuzer, H. J.; Grunze, M. The Role of "Inert" Surface Chemistry in Marine Biofouling Prevention. *Phys. Chem. Chem. Phys.* **2010**, *12*, 4275-4286.
- (15) Brzozowska, A. M.; Parra-Velandia, F. J.; Quintana, R.; Xiaoying, Z.; Lee, S. S. C.; Chin-Sing, L.; Jańczewski, D.; Teo, S. L. M.; Vancso, Biomimicking Micropatterned Surfaces and Their Effect on Marine Biofouling. *Langmuir* **2014**, *30*, 9165-9175.
- (16) Bixler, G. D.; Bhushan, B. Biofouling: Lessons from Nature. *Phil. Trans. R. Soc. A* **2012**, *370*, 2381-2417.
- (17) Rosi, N. L.; Mirkin, C. A. Nanostructures in Biodiagnostics. *Chem. Rev.* **2005**, *105*, 1547-1562.
- (18) Zhou, W.; Jimmy Huang, P.-J.; Ding, J.; Liu, J. Aptamer-Based Biosensors for Biomedical Diagnostics. *Analyst* **2014**, *139*, 2627-2640.

- (19) Coyer, S. R.; García, A. J.; Delamar, E. Facile Preparation of Complex Protein Architectures with Sub-100-nm Resolution on Surfaces. *Angew. Chem. Int. Ed.* **2007**, *46*, 6837-6840.
- (20) Jeyachandran, Y. L.; Terfort, A.; Zharnikov, M. Controlled Modification of Protein-Repelling Self-Assembled Monolayers by Ultraviolet Light: The Effect of the Wavelength. *J. Phys. Chem. C* **2012**, *116*, 9019-9028.
- (21) Weber, T.; Meyerbroeker, N.; Hira, N. K.; Zharnikov, M.; Terfort, A. UV-Mediated Tuning of Surface Biorepulsivity in Aqueous Environment. *Chem. Comm.* **2014**, *50*, 4325-4327.
- (22) Jeyachandran, Y. L.; Meyerbröcker, N.; Terfort, A.; Zharnikov, M. Maskless Ultraviolet Projection Lithography with a Biorepelling Monomolecular Resist. *J. Phys. Chem. C* **2015**, *119*, 494-502.
- (23) Ballav, N.; Terfort, A.; Zharnikov, M. Fabrication of Mixed Self-Assembled Monolayers Designed for Avidin Immobilization by Irradiation Promoted Exchange Reaction. *Langmuir* **2009**, *25*, 9189-9196.
- (24) Ballav, N.; Thomas, H.; Winkler, T.; Terfort, A.; Zharnikov, M. Making Protein Patterns by Writing in a Protein-Repelling Matrix. *Angew. Chem. Int. Ed.* **2009**, *48*, 5833-5836.
- (25) Lee, K.-B.; Park, S.-J.; Mirkin, C. A.; Smith, J. C.; Mrksich, M. Protein Nanoarrays Generated by Dip-Pen Nanolithography. *Science* **2002**, *295*, 1702-1705.
- (26) Lee, K.-B.; Lim, J.-H.; Mirkin, C. A. Protein Nanostructures formed via Direct-Write Dip-Pen Nanolithography. *J. Am. Chem. Soc.* **2003**, *125*, 5588-5589.

(27) Qin, G.; Cai, C. Sub-10-nm Patterning of Oligo(Ethylene Glycol) Monolayers on Silicon Surfaces via Local Oxidation using a Conductive Atomic Force Microscope. *Nanotechnol.* **2009**, *20*, 355306.

(28) Montague, M.; Ducker, R. E.; Chong, K. S. L.; Manning, R. J.; Rutten, F. J. M.; Davies, M. C.; Leggett, G. J. Fabrication of Biomolecular Nanostructures by Scanning Near-Field Photolithography of Oligo(ethylene glycol) Terminated Self-Assembled Monolayers. *Langmuir* **2007**, *23*, 7328-7337.

(29) Alang Ahmad, S. A.; Wong, L. S.; ul-Haq, E.; Hobbs, J. K.; Leggett, G. J.; Micklefield, J. Protein Micro- and Nanopatterning Using Aminosilanes with Protein-Resistant Photolabile Protecting Groups. *J. Am. Chem. Soc.* **2011**, *133*, 2749-2759.

(30) Ul-Haq, E.; Patole, S.; Moxey, M.; Amstad, E.; Vasilev, C.; Hunter, C. N.; Leggett, G. J.; Spencer, N. D.; Williams, N. H. Photocatalytic Nanolithography of Self-Assembled Monolayers and Proteins. *ACS Nano* **2013**, *7*, 7610-7618.

(31) Reynolds, N. P.; Tucker, J. D.; Davison, P. A.; Timney, J. A.; Hunter, C. N.; Leggett, G. J. Site-Specific Immobilization and Micrometer and Nanometer Scale Photopatterning of Yellow Fluorescent Protein on Glass Surfaces. *J. Am Chem. Soc.* **2009**, *131*, 896-897.

(32) Tizazu, G.; el Zubir, O.; Patole, S.; McLaren, A.; Vasilev, C.; Mothersole, D.; Adawi, A.; Hunter, C. N.; Lidzey, D.; Lopez, G.; Leggett, G. Micrometer and Nanometer Scale Photopatterning of Proteins on Glass Surfaces by Photo-degradation of Films Formed from Oligo(Ethylene Glycol) Terminated Silanes. *Biointerphases* **2012**, *7*, 1-9.

(33) Alswieleh, A. M.; Cheng, N.; Canton, I.; Ustbas, B.; Xue, X.; Ladmiral, V.; Xia, S.; Ducker, R. E.; El Zubir, O.; Cartron, M. L.; Hunter, C. N.; Leggett, G. J.; Armes, S. P. Zwitterionic Poly(amino acid methacrylate) Brushes. *J. Am. Chem. Soc.* **2014**, *136*, 9404-9413.

(34) Moxey, M.; Johnson, A.; El-Zubir, O.; Cartron, M.; Dinachali, S. S.; Hunter, C. N.; Saifullah, M. S. M.; Chong, K. S. L.; Leggett, G. J. Fabrication of Self-Cleaning, Reusable Titania Templates for Nanometer and Micrometer Scale Protein Patterning. *ACS Nano* **2015**, *9*, 6262-6270.

(35) Vasilev, C.; Johnson, M. P.; Gonzales, E.; Wang, L.; Ruban, A. V.; Montano, G.; Cadby, A. J.; Hunter, C. N. Reversible Switching between Nonquenched and Quenched States in Nanoscale Linear Arrays of Plant Light-Harvesting Antenna Complexes. *Langmuir* **2014**, *30*, 8481-8490.

(36) Castner, D. G.; Ratner, B. D. Biomedical Surface Science: Foundations to Frontiers. *Surf. Sci.* **2002**, *500*, 28-60.

(37) Langer, R.; Tirrell, D. A. Designing Materials for Biology and Medicine. *Nature* **2004**, *428*, 487-492.

(38) Meyers, S. R.; Grinstaff, M. W. Biocompatible and Bioactive Surface Modifications for Prolonged In Vivo Efficacy. *Chem. Rev.* **2012**, *112*, 1615-1632.

(39) Harris, J. M. *Poly(Ethylene Glycol) Chemistry: Biochemical and Biomedical Applications*; Plenum: New York, 1992.

(40) Prime, K. L.; Whitesides, G. M. Self-Assembled Organic Monolayers: Model Systems for Studying Adsorption of Proteins at Surfaces. *Science* **1991**, *252*, 1164-1167.

- (41) Pale-Grosdemange, C.; Simon, E. S.; Prime, K. L.; Whitesides, G. M. Formation of Self-Assembled Monolayers by Chemisorption of Derivatives of Oligo(Ethylene Glycol) of Structure  $\text{HS}(\text{CH}_2)_{11}(\text{OCH}_2\text{CH}_2)_m\text{OH}$  on Gold. *J. Am. Chem. Soc.* **1991**, *113*, 12-20.
- (42) Lopez, G. P.; Biebuyck, H. A.; Haerter, R.; Kumar, A.; Whitesides, G. M. Fabrication and Imaging of Two-Dimensional Patterns of Proteins Adsorbed on Self-Assembled Monolayers by Scanning Electron Microscopy. *J. Am. Chem. Soc.* **1993**, *115*, 10774-10781.
- (43) Yam, C. M.; Lopez-Romero, J. M.; Gu, J.; Cai, C. Protein-Resistant Monolayers Prepared by Hydrosilylation of  $\alpha$ -Oligo(Ethylene Glycol)- $\omega$ -Alkenes on Hydrogen-Terminated Silicon (111) Surfaces. *Chem. Comm.* **2004**, 2510-2511.
- (44) Hucknall, A.; Rangarajan, S.; Chilkoti, A. In Pursuit of Zero: Polymer Brushes that Resist the Adsorption of Proteins. *Adv. Mater.* **2009**, *21*, 2441-2446.
- (45) Ma, H.; Li, D.; Sheng, X.; Zhao, B.; Chilkoti, A. Protein Resistant Polymer Brushes on Silicon Oxide by Surface Initiated Atom Transfer Radical Polymerization. *Langmuir* **2006**, *22*, 3751-3756.
- (46) Sigal, G. B.; Bamdad, C.; Barberis, A.; Strominger, J.; Whitesides, G. M. A Self-Assembled Monolayer for the Binding and Study of Histidine-Tagged Proteins by Surface Plasmon Resonance. *Anal. Chem.* **1996**, *68*, 490-497.
- (47) Schmid, E. L.; Keller, T. A.; Dienes, Z.; Vogel, H. Reversible Oriented Surface Immobilization of Functional Proteins on Oxide Surfaces. *Anal. Chem.* **1997**, *69*, 1979-1985.

(48) de Groot, G. W.; Demarche, S.; Santonicola, M. G.; Tiefenauer, L.; Vancso, G. J. Smart Polymer Brush Nanostructures Guide the Self-Assembly of Pore-Spanning Lipid Bilayers with Integrated Membrane Proteins. *Nanoscale* **2014**, *6*, 2228-2237.

(49) Falconnet, D.; Pasqui, D.; Park, S.; Eckert, R.; Schiff, H.; Gobrecht, J.; Barbucci, R.; Textor, M. A Novel Approach to produce Protein Nanopatterns by Combining Nanoimprint Lithography and Molecular Self-Assembly. *Nano. Lett.* **2004**, *4*, 1909-1914.

(50) Maury, P.; Escalante, M.; Péter, M.; Reinhoudt, D. N.; Subramaniam, V.; Huskens, J. Creating Nanopatterns of His-Tagged Proteins on Surfaces by Nanoimprint Lithography Using Specific NiNTA-Histidine Interactions. *Small* **2007**, *3*, 1584-1592.

(51) Alvey, R. M.; Biswas, A.; Schluchter, W. M.; Bryant, D. A. Attachment of Noncognate Chromophores to CpcA of *Synechocystis* sp. PCC 6803 and *Synechococcus* sp. PCC 7002 by Heterologous Expression in *Escherichia coli*. *Biochem.* **2011**, *50*, 4890-4902.

(52) Shen, G.; Saunee, N. A.; Williams, S. R.; Gallo, E. F.; Schluchter, W. M.; Bryant, D. A. Identification and characterization of a new class of bilin lyase - The *cpcT* gene encodes a bilin lyase responsible for attachment of phycocyanobilin to CYS-153 on the  $\beta$ -subunit of phycocyanin in *Synechococcus* sp. PCC 7002. *J. Biol. Chem.* **2006**, *281*, 17768-17778.

(53) Zhu, Y.-J.; Olson, N.; Beebe, T. P. Surface Chemical Characterization of 2.5- $\mu$ m Particulates (PM<sub>2.5</sub>) from Air Pollution in Salt Lake City Using TOF-SIMS, XPS, and FTIR. *Env. Sci. Technol.* **2001**, *35*, 3113-3121.

(54) Cheng, F.; Gamble, L. J.; Castner, D. G. XPS, TOF-SIMS, NEXAFS, and SPR Characterization of Nitrilotriacetic Acid-Terminated Self-Assembled Monolayers for Controllable Immobilization of Proteins. *Anal. Chem.* **2008**, *80*, 2564-2573.

(55) Alang-Ahmad, S. A.; Wong, L. S.; ul-Haq, E.; Hobbs, J. K.; Leggett, G. J.; Micklefield, J. Micrometer- and Nanometer-Scale Photopatterning Using 2-Nitrophenylpropyloxycarbonyl-Protected Aminosiloxane Monolayers. *J. Am Chem. Soc.* **2009**, *131*, 1513-1522.

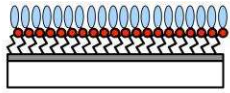
(56) Alang-Ahmad, S. A.; Hucknall, A.; Chilkoti, A.; Leggett, G. J. Patterning by UV-induced Photodegradation of Poly(oligo(ethylene glycol)methacrylate) Brushes. *Langmuir* **2010**, *26*, 9937-9942.

(57) Ducker, R. E.; Janusz, S. J.; Sun, S.; Leggett, G. J. One-Step Photochemical Introduction of Nanopatterned Protein-Binding Functionalities to Oligo(Ethylene Glycol) Terminated Self-Assembled Monolayers. *J. Am Chem. Soc.* **2007**, *129*, 14842-14843.

(58) Prompinit, P.; Achalkumar, A. S.; Han, X.; Bushby, R. J.; Walthi, C.; Evans, S. D. Improved Photoreaction Yields for Soft Ultraviolet Photolithography in Organothiols Self-Assembled Monolayers. *J. Phys. Chem. C* **2009**, *113*, 21642-21647.

(59) Vančik, H. *Aromatic C-nitroso Compounds*; Springer Netherlands, 2013, pp 75 – 76.

TOC GRAPHIC



1. UV
2. Glutaraldehyde
3. NTA / His-protein

